The solution of the hypernetted-chain and Percus–Yevick approximations for fluids of hard spherocylinders

A. Perera, G. Patey

▶ **To cite this version:**

A. Perera, G. Patey. The solution of the hypernetted-chain and Percus–Yevick approximations for fluids of hard spherocylinders. The Journal of Chemical Physics, 1988, 89 (9), pp.5861-5868. 10.1063/1.455537 . hal-04331940

HAL Id: hal-04331940

https://hal.sorbonne-universite.fr/hal-04331940

Submitted on 8 Dec 2023

HAL is a multi-disciplinary open access archive for the deposit and dissemination of scientific research documents, whether they are published or not. The documents may come from teaching and research institutions in France or abroad, or from public or private research centers.

L'archive ouverte pluridisciplinaire **HAL**, est destinée au dépôt et à la diffusion de documents scientifiques de niveau recherche, publiés ou non, émanant des établissements d'enseignement et de recherche français ou étrangers, des laboratoires publics ou privés.

The solution of the hypernetted-chain and Percus–Yevick approximations for fluids of hard spherocylinders

A. Perera and G. N. Patey
Department of Chemistry, University of British Columbia, Vancouver, British Columbia V6T 1Y6, Canada

(Received 22 January 1988; accepted 27 July 1988)

The hypernetted-chain (HNC) and Percus–Yevick (PY) approximations are solved numerically for isotropic fluids of hard spherocylinders with length-to-breadth ratios ranging from 2 to 6. The theoretical results are compared with the available Monte Carlo data for the equation of state and the pair correlation function. The HNC theory was found to predict the existence of a nematic phase at densities in reasonable agreement with recent computer simulations.

I. INTRODUCTION

In a recent[1] paper we have described a general method which can be applied in order to solve the hypernetted-chain (HNC) and Percus–Yevick (PY) integral equation theories for fluids of hard nonspherical particles. Also in Ref. 1 explicit numerical results were presented for fluids of hard ellipsoids of revolution with length-to-breadth ratios a/b varying from 1.25 to 5. Comparison with the available Monte Carlo results[2] strongly indicated that the HNC theory gives a rather good description of the macroscopic properties of this model predicting isotropic–nematic phase changes at densities in good agreement with the Monte Carlo results. The PY approximation, on the other hand, does not give an orientational instability at densities lower than the Monte Carlo freezing transition.

The purpose of the present paper is to describe a similar study carried out for fluids of hard spherocylinders. The HNC and in most cases also the PY equations have been solved for a number of spherocylinders with length-to-breadth ratios varying from $a/b = 2$ to 6 and the equations of state and structural properties are compared with earlier Monte Carlo calculations.[3–7] It is shown that as for ellipsoidal fluids the HNC theory provides a relatively accurate description of spherocylinders in the dense isotropic phase yielding pair correlation functions in good agreement with the available Monte Carlo results. The HNC theory also predicts that the isotropic phase becomes orientationally unstable at densities in reasonable agreement with recent Monte Carlo calculations.[7] In some cases the PY theory gives an equation of state which is more accurate than the HNC approximation but the PY pair correlation functions are generally less accurate than the HNC results. Furthermore, as was the case for hard ellipsoids, the PY approximation does not appear to develop the long-range orientational correlations necessary to destabilize the isotropic phase.

II. THEORY

The pair interaction $u(\mathbf{r},\boldsymbol{\Omega}_1,\boldsymbol{\Omega}_2)$ characterizing fluids of hard nonspherical particles is given by

$$u(\mathbf{r},\boldsymbol{\Omega}_1,\boldsymbol{\Omega}_2) = \begin{cases} \infty, & \text{if particles overlap} \\ 0, & \text{if particles do not overlap} \end{cases}, \quad (1)$$

where $\boldsymbol{\Omega}_1$ and $\boldsymbol{\Omega}_2$ denote sets of Euler angles describing the orientations of particles 1 and 2, and $\mathbf{r} = \mathbf{r}_2 - \mathbf{r}_1$ is a vector joining their centers. In order for Eq. (1) to be of use it is obvious that the minimum contact distance between a pair of particles must be a known function of the particle orientations. This is, of course, the case[3] for the spherocylinders considered in the present paper.

The HNC and PY approximations for hard nonspherical objects are defined by the Ornstein–Zernike (OZ) equation

$$\eta(12) = \frac{\rho}{8\pi^2}\int c(13)[\eta(32) + c(32)]d(3)\,, \quad (2)$$

together with the closure conditions

$$c(12) = \begin{cases} -1 - \eta(12), & \text{if overlap} \\ c_{\mathrm{CL}}(12), & \text{if no overlap} \end{cases}, \quad (3)$$

where $\eta(12) = h(12) - c(12)$,$h(12)$, and $c(12)$ are the pair and direct correlation functions, respectively, ρ is the number density and $d(3) = d\boldsymbol{\Omega}_3\, d\mathbf{r}_3$. In Eq. (3) $c_{\mathrm{CL}}(12)$ denotes the HNC and PY closures which for nonoverlapping pairs can be written in the form

$$c_{\mathrm{HNC}}(12) = h(12) - \ln g(12) \quad (4)$$

and

$$c_{\mathrm{PY}}(12) = 0\,, \quad (5)$$

respectively.

The method of solution of Eqs. (2) and (3) for spherocylinders is analogous to that applied in our earlier work on hard ellipsoids and we will not give the details here. However, in order to introduce the notation it is necessary to indicate that the solutions are obtained by expanding[8,9] the correlation functions in a basis set of rotational invariants, $\Phi^{mnl}_{\mu\nu}(\boldsymbol{\Omega}_1,\boldsymbol{\Omega}_2,\hat{\mathbf{r}})$, defined by

$$\Phi^{mnl}_{\mu\nu}(\boldsymbol{\Omega}_1,\boldsymbol{\Omega}_2,\hat{\mathbf{r}}) = f^{mnl}\sum_{\mu',\nu',\lambda'}\begin{pmatrix} m & n & l \\ \mu' & \nu' & \lambda' \end{pmatrix} \times R^{\,m}_{\mu'\mu}(\boldsymbol{\Omega}_1)R^{\,n}_{\nu'\nu}(\boldsymbol{\Omega}_2)R^{\,l}_{\lambda'0}(\hat{\mathbf{r}})\,, \quad (6)$$

where $\hat{\mathbf{r}}$ is a unit vector in the direction of $\mathbf{r}$, f^{mnl} is a nonzero constant, $R^{\,m}_{\mu'\mu}(\boldsymbol{\Omega})$ is a generalized spherical harmonic,[10] and the large brackets denote the 3-j symbol.[10] Thus, the pair correlation function is given by

 0021-9606/88/215861-08$02.10 © 1988 American Institute of Physics

Downloaded 18 Dec 2001 to 134.157.8.35. Redistribution subject to AIP license or copyright, see http://ojps.aip.org/jcpo/jcpcr.jsp

$$h(12) = \sum_{\substack{mnl \\ \mu\nu}} h_{m\nu}^{mnl}(r)\Phi_{\mu\nu}^{mnl}(12) \quad (7)$$

and the macroscopic quantities of interest such as the Kerr constant can be expressed[1] in terms of the $h_{\mu\nu}^{mnl}(r)$ coefficients.

III. RESULTS

We have investigated fluids of spherocylinders with values of a/b ranging from 2 to 6. The numerical calculations were performed as in Ref. 1. The integral equations were solved by iteration employing 1024 grid points. For $a/b = 2$ and 3 the grid width used was $0.01b$ and this was increased to $0.02b$ for $a/b = 6$. The orientational integrals necessary in the calculation of the $A_{m'n'l'}^{mnl}(r)$ coefficients [cf. Eq. (12b) of Ref. 1] were carried out using Simpson's rule with 81 points. The results reported in this paper were obtained using a basis set which included all terms such that $m,n \leqslant 6$ and $l \leqslant 10$. A few calculations were also carried out with different basis sets (i.e., $m,n,l, \leqslant 6$ and $m,n \leqslant 8$, $l \leqslant 6$) and, although some basis set dependence can be detected at high densities, the qualitative behavior of the thermodynamic and structural properties does not change. The basis set dependence is in fact similar to that found for hard ellipsoids as shown in Figs. 10 and 16 of Ref. 1. The very small scale oscillations discernible in some plots [e.g., Figs. 6(a) and 8(b)] are strongly dependent upon the variables of the numerical solution (i.e., the basis set employed, the number of points used in numerical integrations, etc.) and hence should not be regarded as having physical significance. We emphasize that this comment applies only to the fine "wiggles" and not to the gross structural features discussed in the text.

A. The equation of state

The compressibility factors $\beta P/\rho$, where $\beta = 1/kT$, for fluids of spherocylinders with $a/b = 2,3$, and 6 are plotted in Figs. 1–3. The figures contain HNC and PY results obtained using both the virial and compressibility equations [denoted by (V) and (C), respectively]. The curves given by a density expansion due to Boublik [cf. Eq. (14) of Ref. 11] as well as Monte Carlo results for $a/b = 2,3$ (from Refs. 5 and 6), and 6 (from Ref. 7) are also included.

From Fig. 1 it can be seen that for $a/b = 2$ the present results for spherocylinders follow the pattern previously observed[1] (note erratum) for fluids of hard ellipsoids. That is the PY(C) route provides the best agreement with the Monte Carlo calculations. This is qualitatively similar to the situation for fluids of hard spheres. However, for $a/b = 3$ (cf. Fig. 2) and 6 (cf. Fig. 3) the accuracy of the PY(V) and/or HNC(C) values can equal or better the PY(C) results.

Finally we note that the Boublik expansion which gives very good values for $\beta P/\rho$ at $a/b = 2$ (cf. Fig. 1) is accurate only at low densities for $a/b = 3$ and 6 (cf. Figs. 2 and 3).

B. The pair correlation function

The general expansion (7) for the pair correlation function is defined in terms of the projections $h_{\mu\nu}^{mnl}(r)$. For the present axially symmetric model $\mu = \nu = 0$, and hence for notational simplicity we drop these indices in the following discussion.

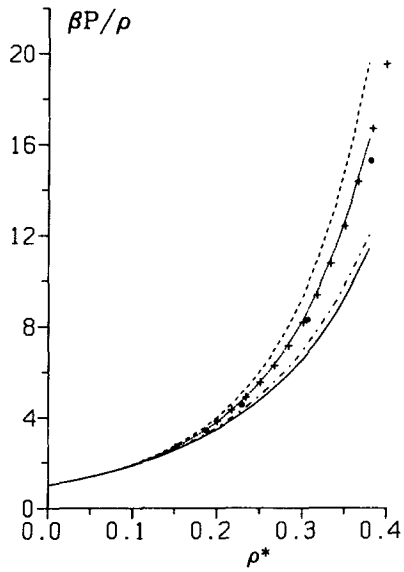

FIG. 1. The compressibility factor for $a/b = 2$. The solid dots represent the Monte Carlo data given in Refs. 5 and 6, and the crosses the density expansion of Boublik (Ref. 11). The solid and dashed curves are the HNC results obtained from the compressibility and virial equations, respectively. The dotted and dash-dot curves are the PY results also obtained with the compressibility and virial equations, respectively.

1. Comparison with Monte Carlo results

Nezbeda[4] has reported some Monte Carlo results for the angle-dependent pair correlation function in fluids of hard spherocylinders. Nezbeda did not expand the pair correlation function as in Eq. (7), but instead in products of spherical harmonics[10] according to the equation

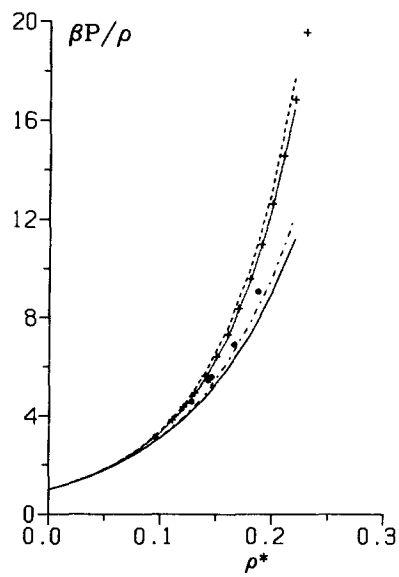

FIG. 2. The compressibility factor for $a/b = 3$. The curves are as in Fig. 1. The Monte Carlo results are from Refs. 5 and 6.

Downloaded 18 Dec 2001 to 134.157.8.35. Redistribution subject to AIP license or copyright, see http://ojps.aip.org/jcpo/jcpcr.jsp

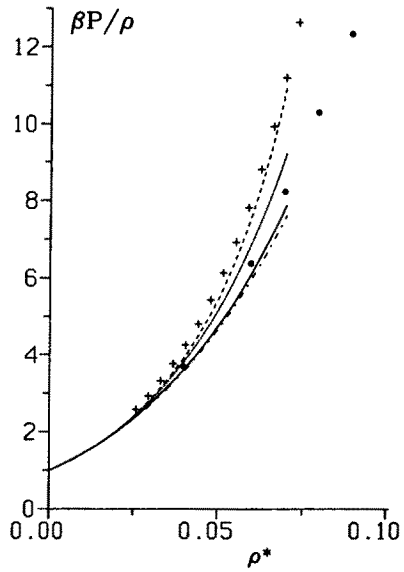

FIG. 3. The compressibility factor for $a/b = 6$. The curves are as in Fig. 1. The Monte Carlo results are from Ref. 7.

$$h(12) = 4\pi \sum_{mn\chi} h^{(N)}_{mn\chi}(r) Y^{\chi}_{m}(\Omega_1) Y^{-\chi}_{n}(\Omega_2) , \tag{8}$$

where we have used the superscript (N) in order to avoid confusing the coefficients in Eq. (8) with those of Eq. (7). In the Appendix it is shown that if

$$f^{mnl} = \sqrt{(2n+1)(2m+1)} , \tag{9}$$

then the $h^{mnl}(r)$ and $h^{(N)}_{mn\chi}$ coefficients are related by real space "χ-transform" pairs.[8,9] We obtain

$$h^{(N)}_{mn\chi}(r) \equiv H^{mn}_{00;\chi}(r) = \sum_{l=|m-n|}^{m+n} \begin{pmatrix} m & n & l \\ \chi & -\chi & 0 \end{pmatrix} h^{mnl}(r) , \tag{10}$$

and the inverse relationship

$$h^{mnl}(r) = (2l+1) \sum_{\chi=-\min(m,n)}^{\min(m,n)} \begin{pmatrix} m & n & l \\ \chi & -\chi & 0 \end{pmatrix} h^{(N)}_{mn\chi}(r) , \tag{11}$$

where $H^{mn}_{\mu\nu;\chi}(r)$ denotes a real space χ transform. The $H^{mn}_{\mu\nu;\chi}(r)$ are analogous to the Fourier space χ transforms introduced by Blum[8(b)] and applied[9] in the resolution of the OZ equation.

Thus given our $h^{mnl}(r)$ projections it is easy to calculate the coefficients obtained by Nezbeda.[4] Of course for the radial distribution function, $g^{000}(r) = h^{000}(r) + 1$ (i.e., the first coefficient) both expansions are equivalent. In addition to $g^{000}(r)$ Nezbeda also reports the coefficients $h^{(N)}_{200}(r)$ and $h^{(N)}_{220}(r)$ which in terms of our projections are explicitly given by the expressions

$$h^{(N)}_{200}(r) = \frac{1}{\sqrt{5}} h^{202}(r) \tag{12}$$

and

$$h^{(N)}_{220}(r) = \frac{1}{\sqrt{5}} h^{220}(r) - \sqrt{\frac{2}{35}} h^{222}(r) + \sqrt{\frac{2}{35}} h^{224}(r) . \tag{13}$$

The HNC and PY curves found for $a/b = 2$ and $\rho^* = 0.2292$, 0.3056, and 0.3820 are compared with Monte Carlo results (the Monte Carlo values were obtained from the curves given in Ref. 4) in Figs. 4(a)–4(c), 5(a)–5(c), and 6(a)–6(c), respectively. From Figs. 4(a)–4(c) it can be seen that at $\rho^* = 0.2292$ the HNC and PY curves are similar

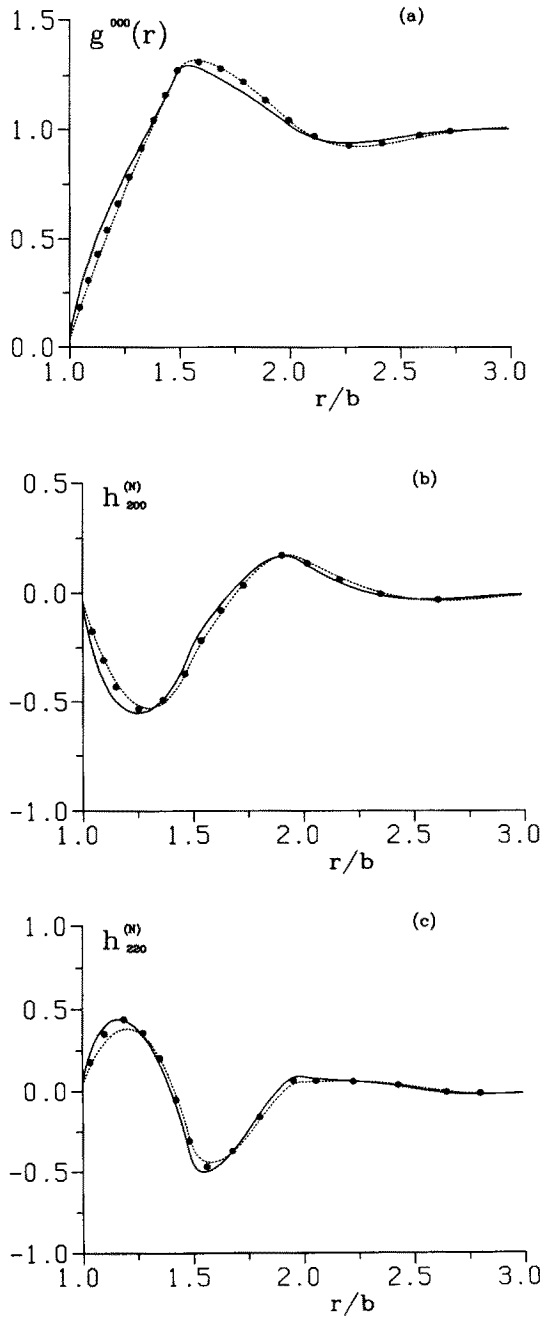

FIG. 4. Comparison with Monte Carlo results (Ref. 4) for (a) $g^{000}(r)$; (b) $h^{(N)}_{200}(r)$; and (c) $h^{(N)}_{220}(r)$ for $a/b = 2$ and $\rho^* = 0.2292$. The solid and dashed curves are the HNC and PY results, respectively. The solid dots are the Monte Carlo values.

Downloaded 18 Dec 2001 to 134.157.8.35. Redistribution subject to AIP license or copyright, see http://ojps.aip.org/jcpo/jcpcr.jsp

and are in good agreement with the Monte Carlo results. At $\rho^* = 0.3056$ [cf. Figs. 5(a)–5(c)] there are significant differences between the HNC and PY results and the HNC theory is clearly superior. At the highest density $\rho^* = 0.3820$ [cf. Figs. 6(a)–6(c)] the HNC curves are still in reasonably good agreement with the Monte Carlo values but some discrepancies are evident particularly in the short-range behavior. For example, the HNC theory gives a small peak in $g^{000}(r)$ near $r/b \approx 1.15$ [cf. Fig. 6(a)] whereas only a shoulder is found in the Monte Carlo curve.

For spherocylinders with $a/b = 3$ Monte Carlo results for the pair correlation function have been reported only for the relatively low density $\rho^* = 0.1432$. These results are compared with the HNC and PY theories in Figs. 7(a)–7(c). It is evident from these figures that the HNC and Monte Carlo curves are in excellent agreement for all three projections. The PY approximation, on the other hand, gives a rather poor description of the short-range behavior.

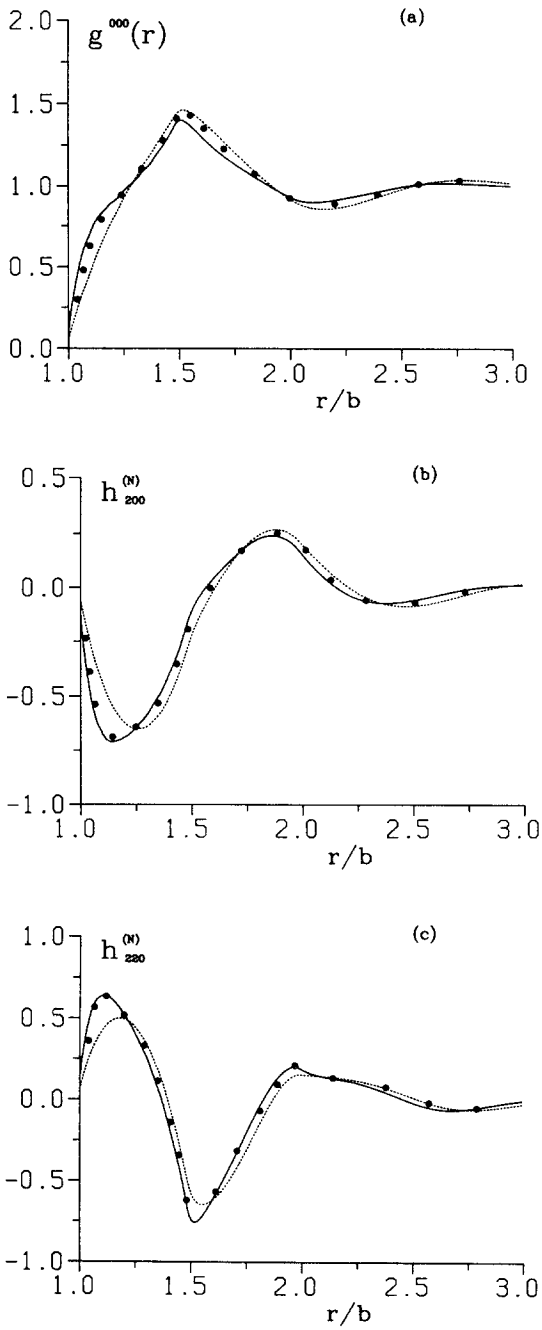

FIG. 5. Comparison with Monte Carlo results (Ref. 4) for (a) $g^{000}(r)$; (b) $h^{(N)}_{200}(r)$; and (c) $h^{(N)}_{220}(r)$ for $a/b = 2$ and $\rho^* = 0.3056$. The curves are as in Fig. 4.

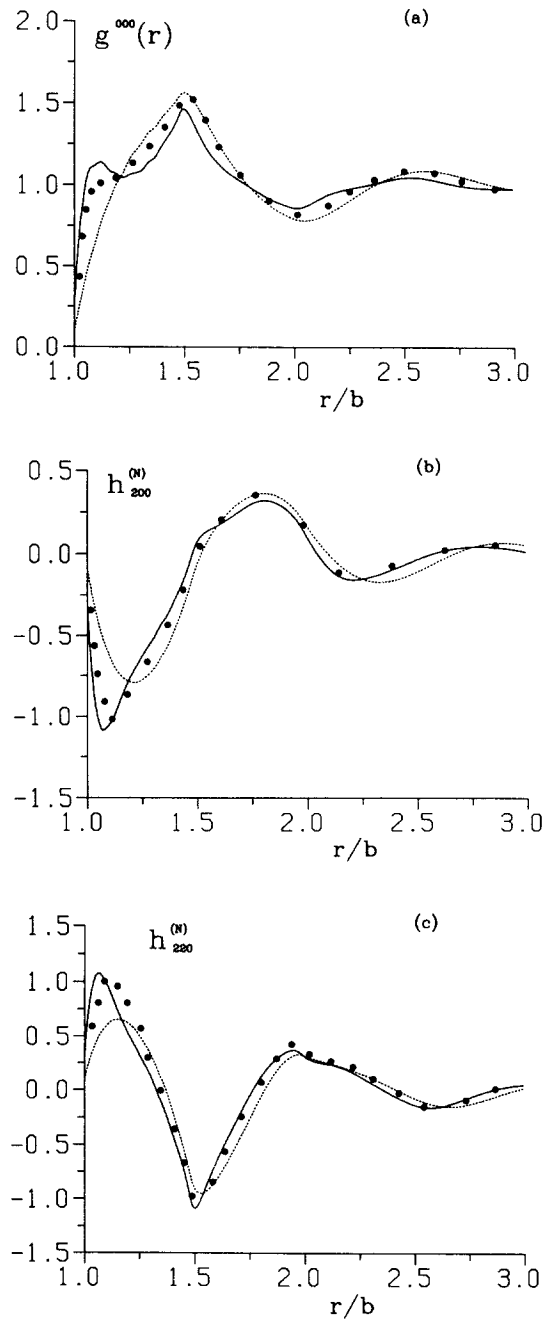

FIG. 6. Comparison with Monte Carlo results (Ref. 4) for (a) $g^{000}(r)$; (b) $h^{(N)}_{200}(r)$; and (c) $h^{(N)}_{220}(r)$ for $a/b = 2$ and $\rho^* = 0.3820$. The curves are as in Fig. 4.

2. The radial distribution function and the structure factor

For $a/b = 2$ the HNC and PY results for $g^{000}(r)$ are compared in Figs. 4(a), 5(a), and 6(a). As noted above,

Downloaded 18 Dec 2001 to 134.157.8.35. Redistribution subject to AIP license or copyright, see http://ojps.aip.org/jcpo/jcpcr.jsp

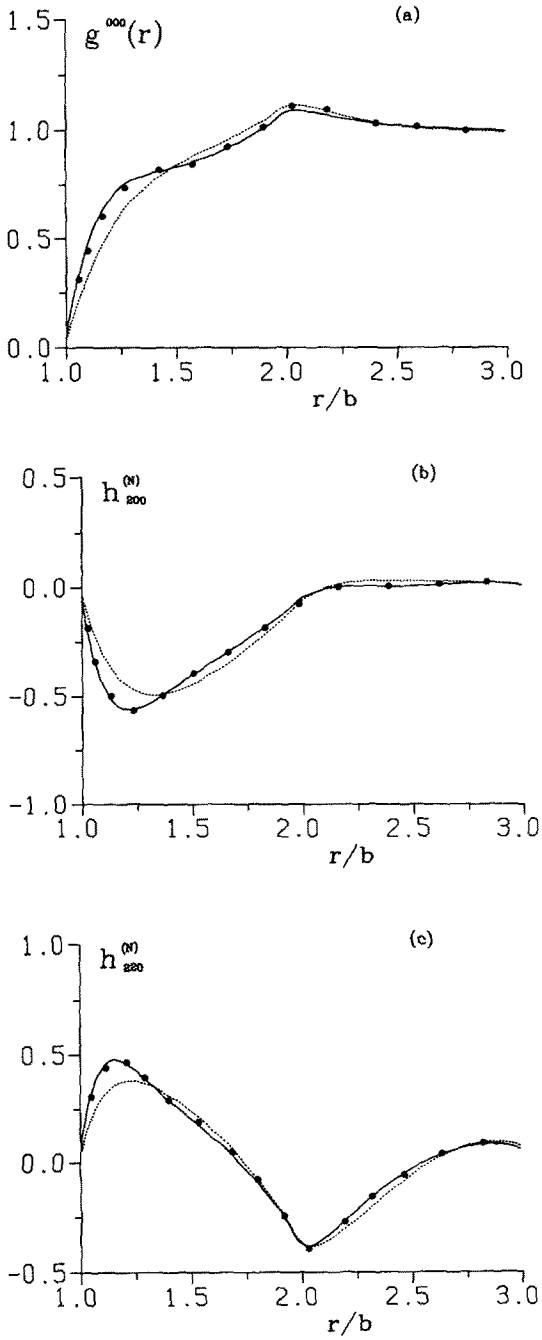

FIG. 7. Comparison with Monte Carlo results (Ref. 4) for (a) $g^{000}(r)$; (b) $h^{(N)}_{200}(r)$; and (c) $h^{(N)}_{220}(r)$ for $a/b = 3$ and $\rho^* = 0.1432$. The curves are as in Fig. 4.

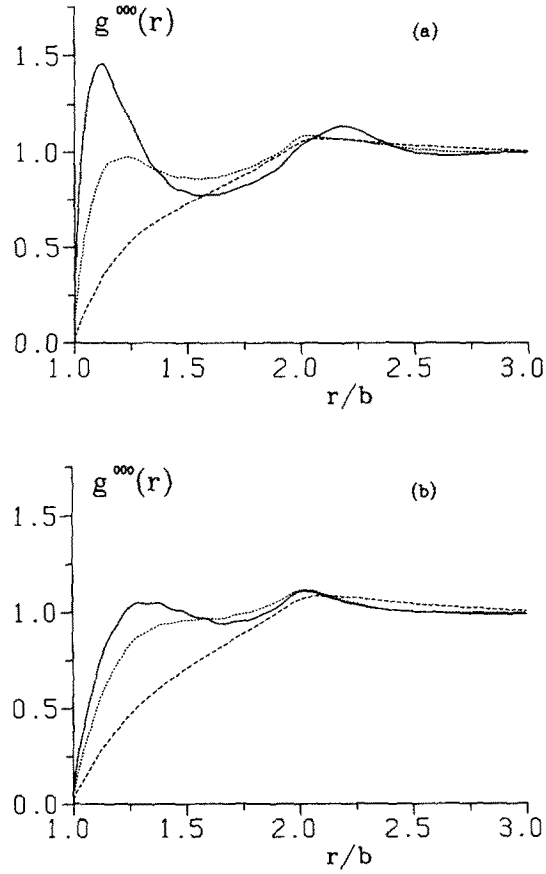

FIG. 8. Radial distribution functions for $a/b = 3$ obtained using the (a) HNC and (b) PY approximations. The dashed, dotted and solid curves are for $\rho^* = 0.1$, 0.19, and 0.23, respectively.

both approximations are similar at low density but differ as ρ^* is increased. Specifically, the HNC curve develops a shoulder and then a peak at $r/b \approx 1.15$ whereas the PY theory does not show this short-range structure rising more or less smoothly to a first maximum at $r/b \approx 1.5$. A shoulder at $r/b \approx 1.15$ was also found in the Monte Carlo calculations.

The HNC and PY radial distribution functions for $a/b = 3$ are compared in Figs. 8(a) and 8(b). It is obvious that the different approximations predict very different results as the density is increased. For example, the HNC curve has a strong distinct peak at $r/b \approx 1.15$ which grows with increasing density whereas the PY result exhibits very little structure. Unfortunately, for $a/b = 3$ there are no Monte Carlo results for $g^{000}(r)$ at high density. Therefore, we cannot conclude with certainty which closure approximation is the more accurate. However, the comparisons made above with Monte Carlo calculations for $a/b = 2$ at high density [cf. Fig. 6(a)] and for $a/b = 3$ at low density [cf. Fig. 7(a)] strongly suggest that the HNC theory is closer to the true result. The HNC and PY results for $a/b = 6$ are shown in Figs. 9(a) and 9(b). Here again at high density the HNC theory gives a relatively sharp peak at short-range whereas the PY curves exhibit only weak structural features.

We remark that at high density the HNC radial distribution functions for spherocylinders are generally more structured than the results obtained for ellipsoids of the same length-to-breadth ratio. Most notably the peak at short range is not so sharp and pronounced for fluids of hard ellipsoids (cf. Fig. 8 of Ref. 1).

The structure factor $S(k)$ is defined by the equation

$$S(k) = 1 + \rho \tilde{h}^{000}(k) , \tag{14}$$

where $\tilde{h}^{000}(k)$ is the Fourier transform of $h^{000}(r)$. The structure factors given by the HNC theory for $a/b = 3$ and 6 are shown in Figs. 10(a) and 10(b). It can be seen that at high density the $S(k)$ have oscillatory structural features which change as a/b is increased. For $a/b = 3$ [cf. Fig. 10(a)]

Downloaded 18 Dec 2001 to 134.157.8.35. Redistribution subject to AIP license or copyright, see http://ojps.aip.org/jcpo/jcpcr.jsp

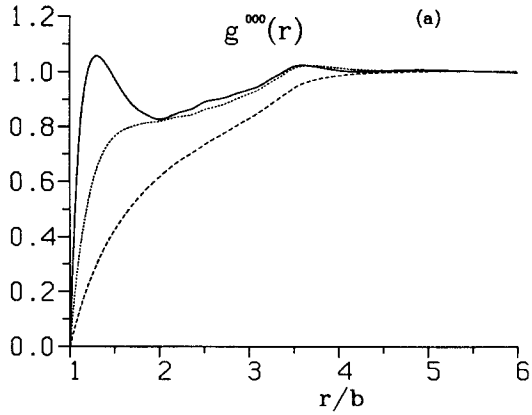

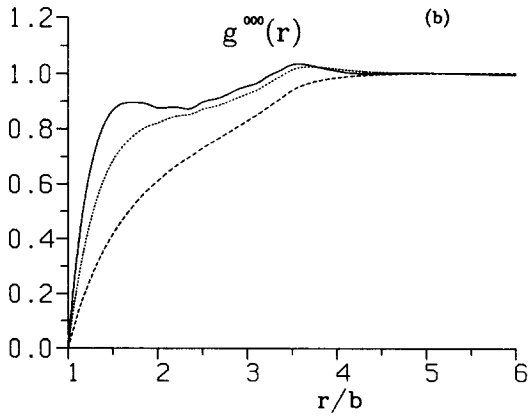

FIG. 9. Radial distribution functions for $a/b = 6$ obtained using the (a) HNC and (b) PY approximations. The dashed, dotted, and solid curves are for $\rho^* = 0.01$, 0.045, and 0.07, respectively.

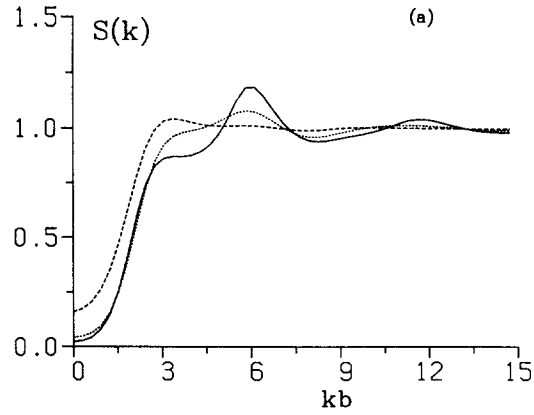

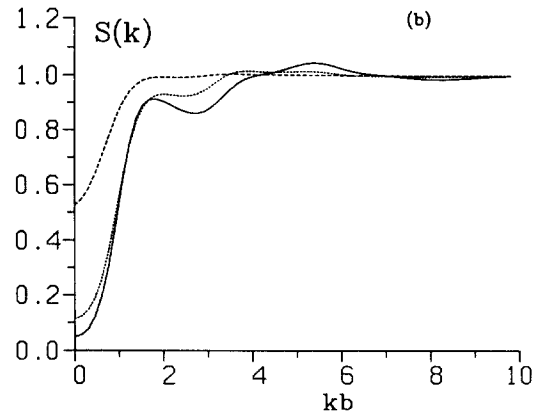

FIG. 10. Structure factors given by the HNC approximation for: (a) $a/b = 3$, the dashed, dotted, and solid curves are HNC results for $\rho^* = 0.1$, 0.19, and 0.23, respectively; (b) $a/b = 6$, the dashed, dotted, and solid curves are HNC results for $\rho^* = 0.01$, 0.045, and 0.07, respectively.

$S(k)$ has a shoulder at $bk \approx 3$ and a peak at $bk \approx 6$. When a/b is increased to 6 [cf. Fig. 10(b)] the shoulder becomes a weak peak. The peak at $bk \approx 6$ decreases in height as a/b increases and is not very pronounced for $a/b = 6$. The Percus–Yevick structure factors are qualitatively similar to the HNC results.

At high density the structure factors for spherocylinders differ significantly from the corresponding results for ellipsoids. In particular, for $a/b = 3$ the ellipsoids give essentially a single peak at $kb \approx 2$ and the oscillatory structure with peaks at $kb \approx 6$, 12, etc. [cf. Fig. 10(a)] is not present (cf. Fig. 12 of Ref. 1). This reflects the differences in the radial distribution functions noted above.

C. Stability of the isotropic phase and the static Kerr constant

For axially symmetric nondipolar particles the static Kerr constant K is given by[1,12,13]

$$K = \beta A \left[1 + \frac{f^{220}}{5^{3/2}} \rho \tilde{h}^{220}(0) \right], \tag{15}$$

where

$$\tilde{h}^{220}(0) = 4\pi \int r^2 h^{220}(r) dr \tag{16}$$

is the value of the Fourier transform $\tilde{h}^{220}(k)$ at $k = 0$, and A is a constant dependent only upon single particle properties. It is shown in Ref. 1 that K can also be expressed in terms of the direct correlation function according to the equation

$$K = \beta A \left[1 - \frac{f^{220}}{5^{3/2}} \rho \tilde{c}^{220}(0) \right]^{-1}, \tag{17}$$

where $\tilde{c}^{220}(0)$ is defined as in Eq. (16).

It can also be shown[1,12,14] that the absolute stability limit of the isotropic relative to the nematic phase is signalled by the divergence of $\tilde{h}^{220}(0)$ or equivalently of K. Thus as the isotropic phase becomes orientationally unstable the inverse Kerr constant $K^{-1} \to 0$. It is important to emphasize that the condition $K^{-1} \to 0$ does not determine the thermodynamic phase transition, but rather a point on the spinodal line. For hard objects this means that the density at which $K^{-1} = 0$ establishes a stability limit in the sense that at higher densities the isotropic phase cannot exist even as a metastable state.

The reduced Kerr constants $\beta A K^{-1}$ for the various fluids studied are plotted in Fig. 11. The curves obtained are obviously very similar to those obtained for fluids of hard ellipsoids (cf. Fig. 17 of Ref. 1). That is for the same value of a/b the HNC curves fall to zero much more rapidly than the PY results. The HNC spinodal points occur at $\rho^* \approx 0.238$

Downloaded 18 Dec 2001 to 134.157.8.35. Redistribution subject to AIP license or copyright, see http://ojps.aip.org/jcpo/jcpcr.jsp

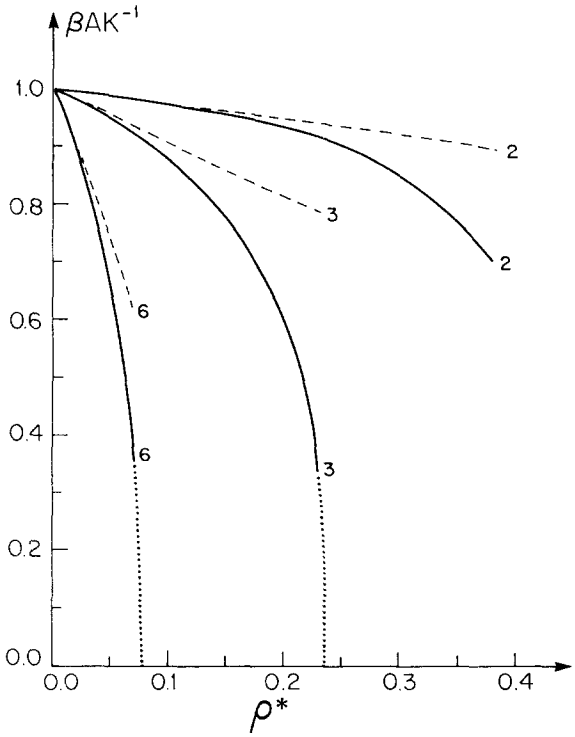

FIG. 11. The reduced inverse Kerr constant as a function of density. The values of a/b for the various curves are indicated on the plot. The calculated and extrapolated HNC curves are represented by solid and dotted lines, respectively. The dashed curves denote the PY results.

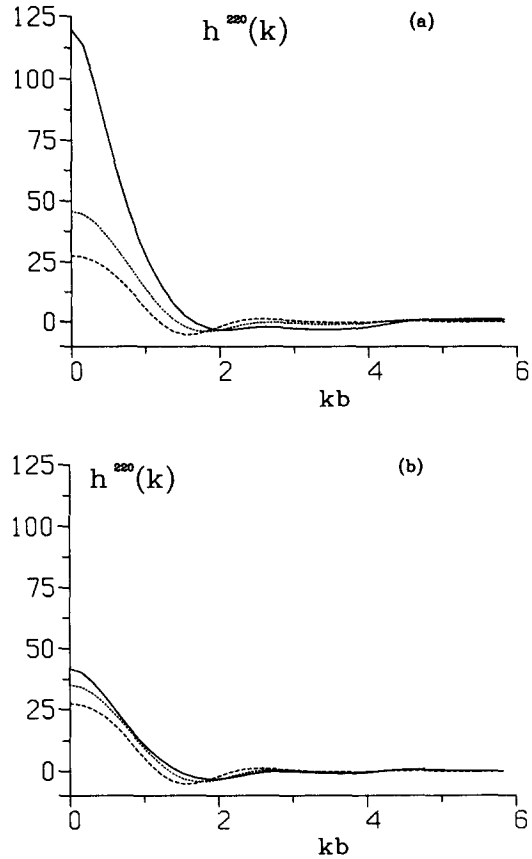

FIG. 12. The Fourier transform $\tilde{h}^{220}(k)$ for $a/b = 6$ obtained using the (a) HNC and (b) PY approximations. The curves are as in Figs. 9.

and 0.079 for $a/b = 3$ and 6, respectively. For $a/b = 3$ the HNC value does not agree with the Monte Carlo calculations of Baron[3] which did not indicate a nematic phase for this system. However, for $a/b = 6$ Frenkel has recently reported[7] an isotropic–nematic transition at $\rho^* \approx 0.089$ which is somewhat higher than the density of the HNC spinodal point. Thus, it appears that the HNC theory predicts that the isotropic phase becomes unstable at densities which are a little lower than the true values.

As previously observed[1] for ellipsoidal systems, the PY theory for spherocylinders (at least for densities where numerical solutions can be obtained) does not appear to develop the long-range orientational correlations necessary to destabilize the isotropic phase. This is illustrated in Figs. 12(a) and 12(b) where we have plotted the HNC and PY results for $\tilde{h}^{220}(k)$ for $a/b = 6$. We note that at low density both theories are very similar but the divergence of $\tilde{h}^{220}(0)$ evident in the HNC curves does not occur in the PY case.

IV. CONCLUSIONS

In this paper we have given numerical results obtained by solving the HNC and PY theories for fluids of hard spherocylinders with length-to-breadth ratios of 2, 3, and 6. Comparisons with existing Monte Carlo data show that for $a/b = 2$, the PY compressibility equation is the most accurate route to the equation of state. However, for the larger values of a/b this is no longer true and other routes [i.e., PY(V) and/or HNC(C)] can yield results of equal or better accuracy.

For $a/b = 2$ and 3, we have compared the radial distribution functions as well as two additional coefficients in the spherical harmonic expansion of $g(12)$ with Monte Carlo results reported by Nezbeda.[4] For these functions the HNC theory is found to be in very good agreement with the Monte Carlo calculations. The PY approximation is less accurate especially at the higher densities.

We have also attempted to locate the stability limit of the isotropic phase by determining the density at which the static Kerr constant diverges. Comparisons with Monte Carlo results indicate that the stability limits given by the HNC theory are about 10% lower than the true values. These observations are consistent with the HNC results for hard ellipsoids. The PY theory, on the other hand, does not produce long-range orientational correlations at densities for which we were able to obtain numerical solutions. Again this is in accord with our earlier calculations for hard ellipsoids.

ACKNOWLEDGMENTS

We thank Dr. D. Frenkel for allowing us to quote his computer simulation results prior to publication. Acknowledgment is made to the Donors of the Petroleum Research Fund, administered by the American Chemical Society, for partial support of this research. We are also grateful for the

Downloaded 18 Dec 2001 to 134.157.8.35. Redistribution subject to AIP license or copyright, see http://ojps.aip.org/jcpo/jcpcr.jsp

financial support of the Natural Sciences and Engineering Research Council of Canada.

APPENDIX: THE DERIVATION OF EQ. (10)

Here we assume that $\Phi_{\mu\nu}^{mnl}(12)$, $h(12)$, and f^{mnl} are as defined by Eqs. (6), (7), and (9), respectively. Then if we choose $\mathbf{r}_{12}$ to be aligned with the laboratory fixed z axis such that

$$R^{\,l}_{\lambda 0}(\hat{\mathbf{r}}_{12}\equiv\hat{\mathbf{z}}) = \delta_{\lambda 0}\ , \tag{A1}$$

and using the properties of the 3-j symbols we obtain

$$h(12) = \sum_{\substack{mnl\\ \mu\nu}} \sum_{\chi=-\min(m,n)}^{\min(m,n)} H^{mn}_{\mu\nu;\chi}(r) \times\sqrt{(2m+1)(2n+1)}\,R^{\,m}_{\chi\mu}(1)R^{\,n}_{-\chi\nu}(2)\ , \tag{A2}$$

where

$$H^{mn}_{\mu\nu;\chi}(r) = \sum_{l=|m-n|}^{m+n} \begin{pmatrix} m & n & l \\ \chi & -\chi & 0 \end{pmatrix} h^{mnl}_{\mu\nu}(r) \tag{A3}$$

is the χ transform of Blum[8(b)] defined in r space. The inverse of Eq. (A3) is given by[8(b)]

$$h^{mnl}_{\mu\nu}(r) = (2l+1) \sum_{\chi=-\min(m,n)}^{\min(m,n)} \begin{pmatrix} m & n & l \\ \chi & -\chi & 0 \end{pmatrix} H^{mn}_{\mu\nu;\chi}(r)\ . \tag{A4}$$

One can check that inserting Eq. (A4) into Eq. (7) leads to Eq. (A2) by using Eq. (A1) and the identity[10]

$$\sum_{l} (2l+1) \begin{pmatrix} m & n & l \\ \chi & -\chi & 0 \end{pmatrix} \begin{pmatrix} m & n & l \\ \mu & -\mu & 0 \end{pmatrix} = \delta_{\chi\mu}\ . \tag{A5}$$

Equation (A2) is a generalization to arbitrary symmetry of an expression often found in the literature[4,6] for axially symmetric molecules. For that particular case $\mu=\nu=0$, and the Wigner matrix elements occuring in Eq. (A2) are given by[10]

$$R^{\,m}_{\chi_0}(1) = \sqrt{\frac{4\pi}{2m+1}}\, Y^{\chi}_{m}(1)\ . \tag{A6}$$

This leads immediately to the result

$$h(12) = 4\pi \sum_{mn\chi} H^{mn}_{00;\chi}(r)\, Y^{\chi}_{m}(1)\, Y^{-\chi}_{n}(2)\ , \tag{A7}$$

from which Eq. (10) can be readily deduced.

[1] A. Perera, P. G. Kusalik, and G. N. Patey, J. Chem. Phys. **87**, 1295 (1987); **89**, 5969 (1988).
[2] D. Frenkel and B. M. Mulder, Mol. Phys. **55**, 1171, 1193 (1985).
[3] J. Vieillard-Baron, Mol. Phys. **28**, 809 (1974).
[4] I. Nezbeda, Czech. J. Phys. B **26**, 1087 (1976).
[5] T. Boublik, I. Nezbeda, and O. Trnka, Czech. J. Phys. B **26**, 1081 (1976).
[6] P. A. Monson and M. Rigby, Chem. Phys. Lett. **58**, 122 (1978).
[7] D. Frenkel (private communication).
[8] (a) L. Blum and A. J. Torruella, J. Chem. Phys. **56**, 303 (1972); (b) L. Blum, *ibid.* **57**, 1862 (1972); **58**, 3295 (1973).
[9] P. Fries and G. N. Patey, J. Chem. Phys. **82**, 529 (1985).
[10] A. Messiah, *Quantum Mechanics* (Wiley, New York, 1962), Vol. II.
[11] T. Boublik, Mol. Phys. **59**, 371 (1986).
[12] A. Perera, P. G. Kusalik, and G. N. Patey, Mol. Phys. **60**, 77 (1987).
[13] S. Kielich, *Dielectric and Related Molecular Process* (Chemical Society of London, London, 1972), Vol. 1, Chap. 7.
[14] J. Stecki and A. Kloczkowski, J. Phys. (Paris) C **3**, 40 (1979); Mol. Phys. **51**, 42 (1981).

Downloaded 18 Dec 2001 to 134.157.8.35. Redistribution subject to AIP license or copyright, see http://ojps.aip.org/jcpo/jcpcr.jsp